Article

Ferromagnetic Ordering in Bisthiaselenazolyl Radicals: Variations on a Tetragonal Theme

Craig M. Robertson, Alicea A. Leitch, Kristina Cvrkalj, Daniel J. T. Myles, Robert W. Reed, Paul A. Dube, and Richard T. Oakley

J. Am. Chem. Soc., **2008**, 130 (44), 14791-14801 • DOI: 10.1021/ja8054436 • Publication Date (Web): 11 October 2008

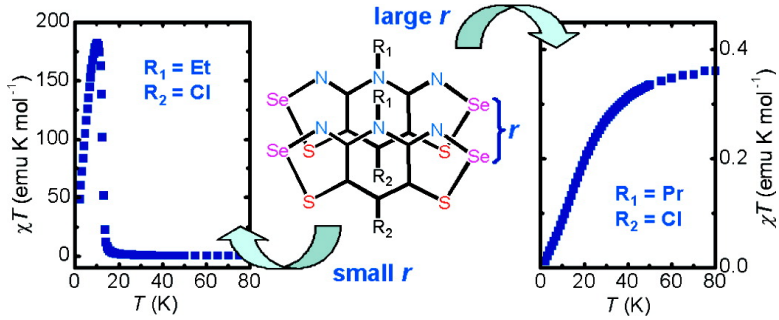

More About This Article

Additional resources and features associated with this article are available within the HTML version:

- Supporting Information
- Access to high resolution figures
- Links to articles and content related to this article
- Copyright permission to reproduce figures and/or text from this article

View the Full Text HTML

J|A|C|S
ARTICLES

Published on Web 10/11/2008

Ferromagnetic Ordering in Bisthiaselenazolyl Radicals: Variations on a Tetragonal Theme

Craig M. Robertson,[†] Alicea A. Leitch,[†] Kristina Cvrkalj,[†] Daniel J. T. Myles,[†] Robert W. Reed,[†] Paul A. Dube,[‡] and Richard T. Oakley*,[†]

Department of Chemistry, University of Waterloo, Waterloo, Ontario N2L 3G1, Canada, and Brockhouse Institute for Materials Research, McMaster University, Hamilton, Ontario L8S 4L8, Canada

Received July 14, 2008; E-mail: oakley@uwaterloo.ca

Abstract: A series of five isostructural bisthiaselenazolyl radicals **2** have been prepared and characterized by X-ray crystallography. The crystal structures, all belonging to the tetragonal space group $P\bar{4}2_1m$, consist of slipped π-stack arrays of undimerized radicals packed about $\bar{4}$ centers running along the *z*-direction, an arrangement which gives rise to a complex lattice-wide network of close intermolecular Se---Se′ contacts. Variations in R_1 (Et, Pr, CH_2CF_3) with R_2 = Cl lead to significant changes in the degree of slippage of the π-stacks and hence the proximity of the Se---Se′ interactions. By contrast, variations in R_2 (Cl, Br, Me) with R_1 = Et induce very little change in either the degree of slippage or the intermolecular contacts. Variable-temperature conductivity (σ) measurements show relatively constant values for the conductivity σ(300 K) (10^{-5}–10^{-4} S cm^{-1}) and thermal activation energy E_{act} (0.27–0.31 eV). Variable-temperature magnetic susceptibility measurements indicate that radicals **2b** and **2c** (R_1 = Pr, CH_2CF_3; R_2 = Cl) behave as weakly antiferromagnetically coupled Curie–Weiss paramagnets, but in **2a**, **2d** and **2e** (R_1 = Et; R_2 = Cl, Me, Br) ferromagnetic ordering is observed, with T_c values of 12.8 (R_2 = Cl), 13.6 (R_2 = Me), and 14.1 K (R_2 = Br). The origin of the dramatically different magnetic behavior across the series has been explored in terms of a direct through-space mechanism by means of DFT calculations on individual pairwise exchange energies. These indicate that antiferromagnetic exchange between radicals along the π-stacks increases with π-stack slippage.

Introduction

The development of molecular conductors and magnetic materials has been dominated by the use of charge transfer (CT) as the means of generating charge and spin carriers. From organic π-donors based on the tetrathiafulvalene (TTF) core and acceptors such as tetracyanoquinodimethane (TCNQ) have emerged a wealth of conductive CT salts.[1,2] The incorporation of transition metal-containing counteranions has allowed for the generation of materials displaying both conductive and magnetic properties.[3] Charge transfer to fullerenes has also provided a wide array of conducting,[4] superconducting,[5,6] and magnetic[7] materials. All of these systems, however, are based on the use of two components, that is, a donor and acceptor, although it is possible to embed the two functions into a single molecule.[8]

The quest for new electronic and magnetic materials based on single-component systems has led to increasing interest in neutral radicals, for in principle the unpaired electron in these systems can serve as a carrier of both charge and spin. The

[†] University of Waterloo.
[‡] McMaster University.

(1) (a) Garito, A. F.; Heeger, A. J. *Acc. Chem. Res.* **1974**, *7*, 232. (b) Torrance, J. B. *Acc. Chem. Res.* **1979**, *12*, 79. (c) Williams, J. M.; Ferraro, J. R.; Thorn, R. J.; Carlson, K. D.; Geiser, U.; Wang, H. H.; Kini, A. M.; Whangbo, M.-H. *Organic Superconductors (Including Fullerenes)*; Prentice Hall: Englewood Cliffs, NJ, 1992.
(2) (a) Bendikov, M.; Wudl, F.; Perepichka, D. F. *Chem. Rev.* **2004**, *104*, 4891. (b) Jérome, D. *Chem. Rev.* **2004**, *104*, 5565. (c) Geiser, U.; Schlueter, J. A. *Chem. Rev.* **2004**, *104*, 5203. (d) Yamada, J.; Akutsu, H.; Nishikawa, H.; Kikuchi, K. *Chem. Rev.* **2004**, *104*, 5057. (e) Saito, G.; Yoshida, Y. *Bull. Chem. Soc. Jpn.* **2007**, *80*, 1.
(3) (a) Coronado, E.; Galán-Mascarós, J. R.; Gómez-García, C. J.; Laukhin, V. *Nature* **2000**, *408*, 447. (b) Coronado, E.; Day, P. *Chem. Rev.* **2004**, *104*, 5419. (c) Coronado, E.; Giménez-Saiz, C.; Gómez-García, C. J. *Coord. Chem. Rev.* **2005**, *249*, 1776. (d) Coronado, E.; Giménez-Saiz, C.; Gómez-García, C. J.; Romero, F. M.; Tarazón, A. *J. Mater. Chem.* **2008**, *18*, 928.
(4) Haddon, R. C.; et al. *Nature* **1991**, *350*, 320.
(5) Hebard, A. F.; Rosseinsky, M. J.; Haddon, R. C.; Murphy, D. W.; Glarum, S. H.; Palstra, T. T. M.; Ramirez, A. P.; Kortan, A. R. *Nature* **1991**, *350*, 600.
(6) Haddon, R. C. *Acc. Chem. Res.* **1992**, *25*, 127.
(7) Allemand, P. M.; Khemani, K. C.; Koch, A.; Wudl, F.; Holczer, K.; Donovan, S.; Gruner, G.; Thompson, J. D. *Science* **1991**, *253*, 301.
(8) (a) Tanaka, H.; Okano, Y.; Kobayashi, H.; Suzuki, W.; Kobayashi, A. *Science* **2001**, *291*, 285. (b) Tanaka, H.; Tokumoto, M.; Ishibashi, S.; Graf, D.; Choi, E. S.; Brooks, J. S.; Yasuzuka, S.; Okano, Y.; Kobayashi, H.; Kobayashi, A. *J. Am. Chem. Soc.* **2004**, *126*, 10518. (c) Kobayashi, A.; Sasa, M.; Suzuki, W.; Fujiwara, E.; Tanaka, H.; Tokumoto, M.; Okano, Y.; Fujiwara, H.; Kobayashi, H. *J. Am. Chem. Soc.* **2004**, *126*, 426. (d) Kobayashi, A.; Fujiwara, E.; Kobayashi, H. *Chem. Rev.* **2004**, *104*, 5243.
(9) (a) Goto, K.; Kubo, T.; Yamamoto, K.; Nakasuji, K.; Sato, K.; Shiomi, D.; Takui, T.; Kubota, M.; Kobayashi, T.; Yakusi, K.; Ouyang, J. *J. Am. Chem. Soc.* **1999**, *121*, 1619. (b) Koutentis, P. A.; Chen, Y.; Cao, Y.; Best, T. P.; Itkis, M. E.; Beer, L.; Oakley, R. T.; Brock, C. P.; Haddon, R. C. *J. Am. Chem. Soc.* **2001**, *123*, 3864. (c) Takano, Y.; Taniguchi, T.; Isobe, H.; Kubo, T.; Morita, Y.; Yamamoto, K.; Nakasuji, K.; Takui, T.; Yamaguchi, K. *J. Am. Chem. Soc.* **2002**, *124*, 11122. (d) Beer, L.; Mandal, S. K.; Reed, R. W.; Oakley, R. T.; Tham, F. S.; Donnadieu, B.; Haddon, R. C. *Cryst. Growth Des.* **2007**, *7*, 101. (e) Beer, L.; Reed, R. W.; Robertson, C. M.; Oakley, R. T.; Tham, F. S.; Haddon, R. C. *Org. Lett.* **2008**, *10*, 3121.

design of stable radicals for use as molecular conductors and as magnetic materials has, however, evolved along separate, seemingly nonconverging paths. Work on conductors has focused on (i) radicals such as phenalenyls[9] and spiro-conjugated biphenalenyls,[10] which possess extensive spin delocalization and, as a consequence, a low onsite Coulomb barrier (U), and/or (ii) radicals containing heavy heteroatoms (sulfur, selenium), which increase intermolecular overlap and hence bandwidth (W),[9d,e,11] the metallic criterion being $W > U$. By contrast, most magnetic materials have been built using light heteroatom radicals such as nitroxyls, nitronyl nitroxides, verdazyls,[12,13] and dithiadiazoyls,[14,15] in which spin density is more localized. In the case of dithiadiazolyls, steric bulk must be employed to suppress dimerization. This combination of spin localization, which increases U, and molecular bulk, which decreases W, militates against the use of these materials as molecular conductors.

In order to improve the conductivity of heteroatom radical-based materials, we have pursued the design of more delocalized (low U) radicals, such as resonance-stabilized bisdithiazolyls **1** (Chart 1).[16−18] The estimated gas-phase disproportionation enthalpies ΔH_{disp} and cell potentials E_{cell} for these materials suggest a reduced value for U in the solid state,[19] but their slipped π-stack structures give rise to reduced bandwidths (W < 0.5 eV).[20] As a result, the materials are Mott insulators;[21]

Chart 1

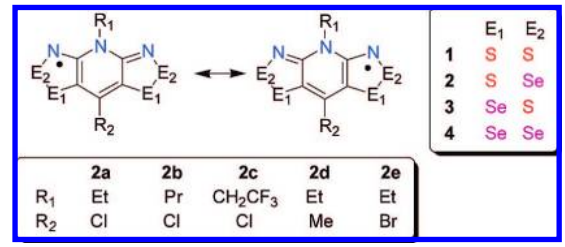

their conductivities (σ) remain activated, with thermal activation energies E_{act} of 0.4−0.5 eV and σ(300 K) values near 10^{-6} S cm^{-1}.

In an attempt to improve the bandwidth and conductivity of **1**, we have investigated the replacement of sulfur by its heavier congener selenium, ideally to afford **2**, **3**, and **4** as an isostructural set that would allow for a direct comparison of the effect of the incorporation of selenium on transport properties. Initial studies on derivatives of **2** (R_1 = Me, Et; R_2 = H) indicated that the radicals dimerized,[22] as indeed do most selenazyl radicals,[23,24] but later work showed that radical association could be avoided by judicious choice of ligands R_1 and R_2.[25] Synthetic routes to **3** and **4** have since been established, from which it has been confirmed that (i) isostructural mapping is possible and (ii) replacement of sulfur by selenium does indeed lead to an improvement in conductivity.[26] What also emerged from these studies was the realization that the incorporation of the heavy heteroatom enhances not only charge transport but also magnetic exchange interactions. Radicals **3** (R_1 = Et; R_2 = H, Cl) and **4** (R_1 = Et; R_2 = H), for example, behave as spin-canted antiferromagnets with ordering temperatures (T_c) of 18, 14, and 27 K, respectively, while **2** and **4** (R_1 = Et; R_2 = Cl) order as ferromagnets with T_c values of 12.8 and 17.0 K.[27,28]

(10) (a) Chi, X.; Itkis, M. E.; Patrick, B. O.; Barclay, T. M.; Reed, R. W.; Oakley, R. T.; Cordes, A. W.; Haddon, R. C. *J. Am. Chem. Soc.* **1999**, *121*, 10395. (b) Mandal, S. K.; Samanta, S.; Itkis, M. E.; Jensen, D. W.; Reed, R. W.; Oakley, R. W.; Tham, F. S.; Donnadieu, B.; Haddon, R. C. *J. Am. Chem. Soc.* **2006**, *128*, 1982.

(11) (a) Cordes, A. W.; Haddon, R. C.; Oakley, R. T. *Adv. Mater.* **1994**, *6*, 798. (b) Cordes, A. W.; Haddon, R. C.; Oakley, R. T. In *The Chemistry of Inorganic Ring Systems*; Steudel, R., Ed.; Elsevier: Amsterdam, 1992, 295. (c) Rawson, J. M.; Alberola, A.; Whalley, A. *J. Mater. Chem.* **2006**, *16*, 2560.

(12) (a) Kinoshita, M.; Turek, P.; Tamura, M.; Nozawa, K.; Shiomi, D.; Nakazawa, Y.; Ishikawa, M.; Takahashi, M.; Awaga, K.; Inabe, T.; Maruyama, Y. *Chem. Lett.* **1991**, 1225. (b) Chiarelli, R.; Novak, M. N.; Rassat, A.; Tholence, J. L. *Nature* **1993**, *363*, 147. (c) Mito, M.; Nakano, H.; Kawae, T.; Hitaka, M.; Takagi, S.; Deguchi, H.; Suzuki, K.; Mukai, K.; Takeda, K. *J. Phys. Soc. Jpn.* **1997**, *66*, 2147. (d) Blundell, S. J. *Contemp. Phys.* **2007**, *48*, 275.

(13) Mito, M.; Nakano, H.; Kawae, T.; Hitaka, M.; Takagi, S.; Deguchi, H.; Suzuki, K.; Mukai, K.; Takeda, K. *J. Phys. Soc. Jpn.* **1997**, *66*, 2147.

(14) Banister, A. J.; Bricklebank, N.; Lavender, I.; Rawson, J. M.; Gregory, C. I.; Tanner, B. K.; Clegg, W.; Elsegood, M. R. J.; Palacio, F. *Angew. Chem., Int. Ed. Engl.* **1996**, *35*, 2533.

(15) Alberola, A.; Less, R. J.; Pask, C. M.; Rawson, J. M.; Palacio, F.; Oliete, P.; Paulsen, C.; Yamaguchi, A.; Farley, R. D.; Murphy, D. M. *Angew. Chem., Int. Ed.* **2003**, *42*, 4782.

(16) Cordes, A. W.; Haddon, R. C.; Oakley, R. T. *Phosphorus, Sulfur, Silicon, Relat. Elem.* **2004**, *179*, 673.

(17) (a) Beer, L.; Brusso, J. L.; Cordes, A. W.; Haddon, R. C.; Itkis, M. E.; Kirschbaum, K.; MacGregor, D. S.; Oakley, R. T.; Pinkerton, A. A.; Reed, R. W. *J. Am. Chem. Soc.* **2002**, *124*, 9498. (b) Beer, L.; Brusso, J.; Cordes, A. W.; Haddon, R. C.; Godde, E.; Itkis, M. E.; Oakley, R. T.; Reed, R. W. *Chem. Commun.* **2002**, 2562. (c) Beer, L.; Britten, J. F.; Brusso, J. L.; Cordes, A. W.; Haddon, R. C.; Itkis, M. E.; MacGregor, D. S.; Oakley, R. T.; Reed, R. W.; Robertson, C. M. *J. Am. Chem. Soc.* **2003**, *125*, 14394.

(18) Beer, L.; Britten, J. F.; Clements, O. P.; Haddon, R. C.; Itkis, M. E.; Matkovich, K. M.; Oakley, R. T.; Reed, R. W. *Chem. Mater.* **2004**, *16*, 1564.

(19) ΔH_{disp} is the enthalpy change for the conversion of two gas-phase radicals R into a cation/anion pair, i.e., $2R \rightleftarrows R^+ + R^-$, and is equal to the difference between the ionization potential (IP) and electron affinity (EA). The cell potential $E_{cell} = E_{1/2}(ox) - E_{1/2}(red)$ is the difference between the half-wave potentials for the oxidation and reduction processes.

(20) More directly superimposed structures with increased bandwidth and conductivity have been achieved, but at a cost of dimerization. See: Leitch, A. A.; Reed, R. W.; Robertson, C. M.; Britten, J. F.; Yu, X.; Secco, R. A.; Oakley, R. T. *J. Am. Chem. Soc.* **2007**, *129*, 7903.

(21) (a) Mott, N. F. *Metal-insulator Transitions*; Taylor and Francis: London, 1990. (b) Whangbo, M.-H. *J. Chem. Phys.* **1979**, *70*, 4963.

(22) (a) Beer, L.; Brusso, J. L.; Haddon, R. C.; Itkis, M. E.; Leitch, A. A.; Oakley, R. T.; Reed, R. W.; Richardson, J. F. *Chem. Commun.* **2005**, 1543. (b) Beer, L.; Brusso, J. L.; Haddon, R. C.; Itkis, M. E.; Kleinke, H.; Leitch, A. A.; Oakley, R. T.; Reed, R. W.; Richardson, J. F.; Secco, R. A.; Yu, X. *J. Am. Chem. Soc.* **2005**, *127*, 18159.

(23) (a) Cordes, A. W.; Haddon, R. C.; Oakley, R. T.; Schneemeyer, L. F.; Waszczak, J. V.; Young, K. M.; Zimmerman, N. M. *J. Am. Chem. Soc.* **1991**, *113*, 582. (b) Andrews, M. P.; et al. *J. Am. Chem. Soc.* **1991**, *113*, 3559. (c) Cordes, A. W.; Haddon, R. C.; Hicks, R. G.; Oakley, R. T.; Palstra, T. T. M.; Schneemeyer, L. F.; Waszczak, J. V. *J. Am. Chem. Soc.* **1992**, *114*, 1729. (d) Britten, J. F.; Clements, O. P.; Cordes, A. W.; Haddon, R. C.; Oakley, R. T.; Richardson, J. F. *Inorg. Chem.* **2001**, *40*, 6820. (e) Beer, L.; Cordes, A. W.; Myles, D. J. T.; Oakley, R. T.; Taylor, N. J. *Cryst. Eng. Chem.* **2000**, *2*, 109. (f) Oakley, R. T.; Reed, R. W.; Cordes, A. W.; Craig, S. L.; Graham, S. B. *J. Am. Chem. Soc.* **1987**, *109*, 7745. (g) Bryan, C. D.; Cordes, A. W.; Oakley, R. T.; Spence, R. E. v. H. *Acta Crystallogr. C* **1995**, *51*, 2402. (h) Cordes, A. W.; Glarum, S. H.; Haddon, R. C.; Hallford, R.; Hicks, R. G.; Kennepohl, D. K.; Oakley, R. T.; Palstra, T. T. M.; Scott, S. R. *J. Chem. Soc., Chem. Commun.* **1992**, 1265.

(24) (a) Feeder, N.; Less, R. J.; Rawson, J. M.; Oliete, P.; Palacio, F. *Chem. Commun.* **2000**, 2449. (b) Parvez, M.; Boeré, R. T. *Acta Crystallogr. C* **1995**, *51*, 2118.

(25) (a) Brusso, J. L.; Derakhshan, S.; Itkis, M. E.; Kleinke, H.; Haddon, R. C.; Oakley, R. T.; Reed, R. W.; Richardson, J. F.; Robertson, C. M.; Thompson, L. K. *Inorg. Chem.* **2006**, *45*, 10958. (b) Beer, L.; Brusso, J. L.; Haddon, R. C.; Itkis, M. E.; Oakley, R. T.; Reed, R. W.; Richardson, J. F.; Secco, R. A.; Yu, X. *Chem. Commun.* **2005**, 5745.

(26) Brusso, J. L.; Cvrkalj, K.; Leitch, A. A.; Oakley, R. T.; Reed, R. W.; Robertson, C. M. *J. Am. Chem. Soc.* **2006**, *128*, 15080.

(27) Leitch, A. A.; Brusso, J. L.; Cvrkalj, K.; Reed, R. W.; Robertson, C. M.; Dube, P. A.; Oakley, R. T. *Chem. Commun.* **2007**, 3368.

Scheme 1

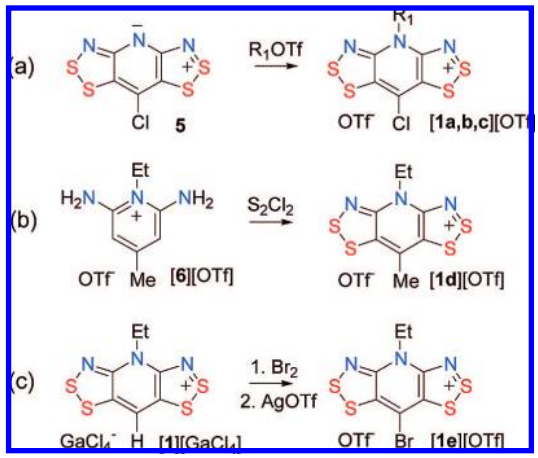

In order to explore the origin of the ferromagnetic response observed in **2** (R_1 = Et; R_2 = Cl; hereafter termed **2a**), we have sought to probe the effect, on structure and transport properties, of minor structural modifications of its molecular framework. Our intent was to make changes that were sufficiently small to preserve the tetragonal ($P\bar{4}2_1m$) space group and solid-state packing pattern found for **2a**. At the same time, however, we hoped to induce changes in intermolecular contacts, and hence overlap and exchange interactions, that would have an effect on magnetic behavior. In essence, we wished to see if we could switch "on" and "off" the ferromagnetic ordering found for **2a** by molecular modification. To that end we synthesized and structurally characterized the series of radicals **2b**−**e**, in which the R_1 and R_2 groups are similar in size to those in **2a**. We have found that all four variants do indeed crystallize in the same tetragonal ($P\bar{4}2_1m$) space group as **2a**, and all show room-temperature conductivities σ(300 K) that are similar to that found for **2a** (near 10^{-4} S cm^{-1}). The magnetic response of the four variants is, however, very different. While **2d** and **2e** behave as ferromagnets, with ordering temperatures (T_c) and coercive fields (H_c) close to those found for **2a**, compounds **2b** and **2c** show no sign of magnetic ordering and instead behave as Curie−Weiss paramagnets with small antiferromagnetic Weiss constants (θ). The origins of this magnetic dichotomy have been explored in terms of a direct through-space mechanism, using density functional theory (DFT) methods to estimate magnetic exchange energies between nearest neighbor radicals.

Results and Discussion

Synthesis. Preparative routes to salts of the all-sulfur framework of **1** were based on double Herz cyclization methods developed in our laboratory.[17,18] Thus, the triflate (trifluoromethanesulfonate) salts of [**1a**,**b**,**c**]$^+$ were obtained by reacting the zwitterion **5**[29] with an alkyl triflate, R_1OTf (R_1 = Et, Pr, CH_2CF_3), as in Scheme 1a. Compound [**1d**][OTf] (Scheme 1b) was prepared by heating sulfur monochloride with [**6**][OTf], itself made by the reaction of *N*-ethyl-2,6-dichloro-4-methylpyridinium triflate with ammonia gas,[18] and compound [**1e**][OTf] was prepared by bromination of the known compound [**1**][$GaCl_4$] (R_1 = Et; R_2 = H),[17] followed by metathesis of the resulting bromide salt with silver triflate, as in Scheme 1c.

Scheme 2

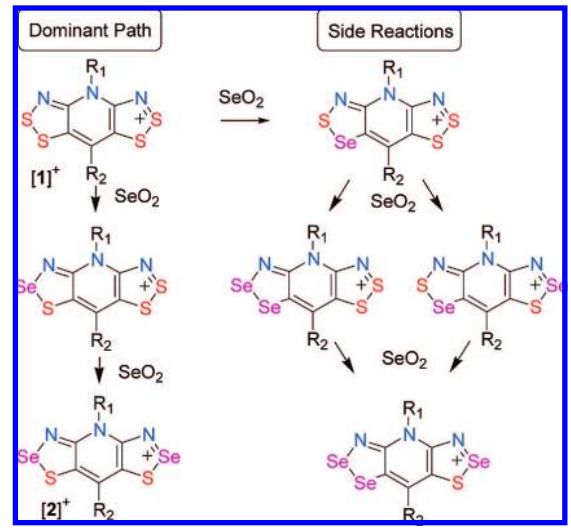

Our initial approach for the generation of derivatives of **2** was based on the condensation of *S*-acetylated pyridinedithiols with selenium halides,[22] which provided an effective but somewhat lengthy preparative procedure. More recently we have taken advantage of chemistry developed 30 years ago[30] for the direct incorporation of selenium into the 2-position of monofunctional 1,2,3-dithiazolylium (DTA) salts using SeO_2 in acetic acid (HOAc) at reflux.[31] The method is readily applicable to the present bifunctional systems and allows for the introduction of selenium into salts of [**1**]$^+$, thereby affording salts of [**2**]$^+$ in a single step. We have used this route previously,[25] and it works well for the preparation of [**2d**]$^+$, which is obtained after 70 min in refluxing HOAc. However, while the approach is simple and fast, when R_2 = Cl, Br, as in [**1a**,**b**,**c**,**e**]$^+$, the harsh reaction conditions originally prescribed lead to selenium insertion which is not regiospecific. Electrospray ionization mass spectrometric (ESI-MS) analysis of the product mixture generated by heating triflate salts of [**1a**,**b**,**c**,**e**]$^+$ with SeO_2 in refluxing HOAc indicated the presence of over 90% S_2Se_2-based cations, but also small amounts of S_3Se_1, S_1Se_3, and even Se_4 materials.

Our interpretation of these observations is that, while the dominant reaction pathway (Scheme 2) involves successive selenium insertion into the 2-position of the heterocycle to afford the desired cation [**2**]$^+$, replacement of sulfur in the 1-position can also take place. From this side product, single and double replacement at either of the two available 2-positions can then occur to give two undesired S_2Se_2 isomers as well as S_1Se_3 materials. Fortunately, full regiospecificity was eventually obtained for [**2a**,**b**,**c**,**e**]$^+$ by performing the SeO_2 insertion in acetonitrile (MeCN) at 110 °C in a glass pressure vessel. Progress of the reaction was monitored by ESI-MS, with complete conversion (99%+) to S_2Se_2 material being achieved in under 72 h. Infrared analysis of the isolated triflates showed clean signatures for the presence of a single regioisomer, that is, [**2**][OTf].

(28) (a) Robertson, C. M.; Myles, D. J. T.; Leitch, A. A.; Reed, R. W.; Dooley, B. M.; Frank, N. L.; Dube, P. A.; Thompson, L. K.; Oakley, R. T. *J. Am. Chem. Soc.* **2007**, *129*, 12688. (b) Robertson, C. M.; Leitch, A. A.; Reed, R. W.; Dube, P. A.; Oakley, R. T. *J. Am. Chem. Soc.* **2008**, *130*, 8414.
(29) Beer, L.; Cordes, A. W.; Oakley, R. T.; Mingie, J. R.; Preuss, K. E.; Taylor, N. J. *J. Am. Chem. Soc.* **2000**, *122*, 7602.
(30) Akulin, Y. I.; Gel'mont, M. M.; Strelets, B. Kh.; Efros, L. S. *Khim. Geterotsikl. Soedin.* **1978**, 912.
(31) A similar approach has been used to incorporate selenium into dithiadiazolylium salts. For example, see: Less, R. J.; Rawson, J. M.; Jones, M. *Polyhedron* **2001**, *20*, 523.

Table 1. Electrochemical Data[a]

radical	$E_{1/2}^{-1/0}$	$E_{1/2}^{0/+1}$	$E_{1/2}^{+1/+2}$	E_{cell}[b]
2a	−0.731	0.013	1.343	0.744
2b	−0.717[c]	0.007	1.331	0.689[d]
2c	−0.619	0.079	1.435	0.698
2d	−0.830	−0.127	1.219	0.703
2e	−0.770[c]	−0.002	1.330	0.730[d]

[a] $E_{1/2}$ values (V) in MeCN, referenced to SCE. [b] $E_{cell} = E_{1/2}^{0/+1} - E_{1/2}^{-1/0}$. [c] Irreversible behavior; E_{pc} value quoted. [d] E_{cell} estimated as $E_{pc}^{0/+1} - E_{pc}^{-1/0}$.

Reduction of the salts [**2a**−**e**][OTf] to the respective radicals in a form suitable for crystallographic work and bulk transport property measurements required careful consideration of the relevant half-wave potentials $E_{1/2}^{(0/+1)}$ (Table 1). These were obtained by cyclic voltammetry measurements on solutions of the salts in MeCN, using 0.1 M *n*-Bu_4NPF_6 as supporting electrolyte. For the more electronegative radicals, that is, those with a halogen occupying the R_2 position, as in **2a**,**b**,**c**,**e**, chemical reduction could be effected with octamethylferrocene (OMFc), hexamethylferrocene (HMFc), or *N*,*N*,*N*′,*N*′-tetramethyl-*p*-phenylenediamine (TMPDA),[28b] but when R_2 = Me,[18] as in **2d**, OMFc or decamethylferrocene (DMFc) was required.

Crystallography. As desired, the four new radicals **2b**−**e** are isostructural with **2a**, all crystallizing in the tetragonal space group $P\bar{4}2_1m$. Unit cell information and crystal metrics, derived from X-ray data collected at ambient temperature, are presented in Table 2. Data sets were also collected at 100 K, and unit cell and structural information from these refinements are available in the Supporting Information. At the molecular level, the crystal structures consist of undimerized radicals bisected by mirror planes; comparative views of the five radicals, specifying atom numbering, are shown in Figure 1. The intramolecular distances and angles are typical for this class of heterocyclic radical, the internal Se1−S1, Se1−N1, and C2−S1 bonds being slightly longer than in the corresponding cations. The difference can be ascribed to the antibonding nature of the radical SOMO, which is not occupied in the cation.[17]

While the crystal structures of the four radicals are essentially identical, there are subtle variations within the series that give rise to major differences in the transport properties described below. The radicals pack in slipped π-stack arrays running along the *z*-direction. The unit cell of the parent radical **2a**, viewed parallel to *c*, and the slipped π-stacks, viewed perpendicular to *c*, are shown in Figure 2. The mean interplanar separations δ between radicals along the π-stacks and the inclination angle τ of the mean molecular plane with respect to the stacking axis are listed in Table 2. As will become apparent, the most significant difference in the five structures is revealed in the value of τ, variations in which are illustrated in Figure 3, which shows the cross-braced nature of adjacent π-stacks, viewed parallel to {1,1,0}. As may be seen, the "butterfly wing" angle 2τ holds steady in the range 115.9°−117.6° in **2a**, **2d**, and **2e**, where R_1 = Et. By contrast, in **2b** (R_1 = Pr) and **2c** (R_1 = CH_2CF_3), the radicals tip more sharply to relieve steric congestion associated with the larger R_1 groups, giving rise to butterfly wing angles 2τ of 100.0° and 107.7°, respectively.

The π-stacks are packed about the $\bar{4}$ centers which run along the *z*-direction, thereby generating stacked clusters linked by intermolecular Se---Se′ contacts *d*1 and *d*2 which, when propagated along the *z*-direction, produce an alternating sequence of Se_4 tetrahedra (Figure 4). In all five structures **2a**−**e**, the values of *d*1 and *d*2 (Table 2) are well within the van der Waals contact (3.8 Å) for two seleniums.[32] However, the three radicals with R_1 = Et (**2a**, **2d**, and **2e**) are associated with *d*1 and *d*2 values that are significantly shorter than those seen in **2b** and **2c**, where bulkier R_1 groups (Pr and CH_2CF_3) are present. There is a third Se---Se′ interaction, denoted as *d*3 in Figure 4 and Table 2, associated with the stacked Se_4 tetrahedra. In all the radicals, this head-to-head contact, which bridges molecules related by a 2-fold axis on either side of the $\bar{4}$ centers, is significantly longer than *d*1 and *d*2. As a result, its direct impact

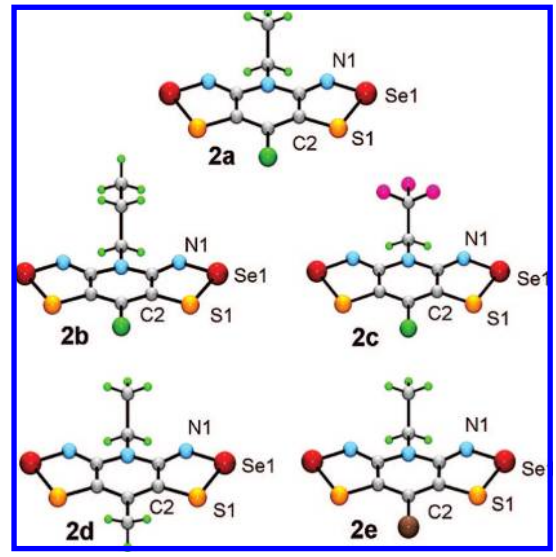

Figure 1. Molecular structures of **2a**−**e**, with atom numbering scheme.

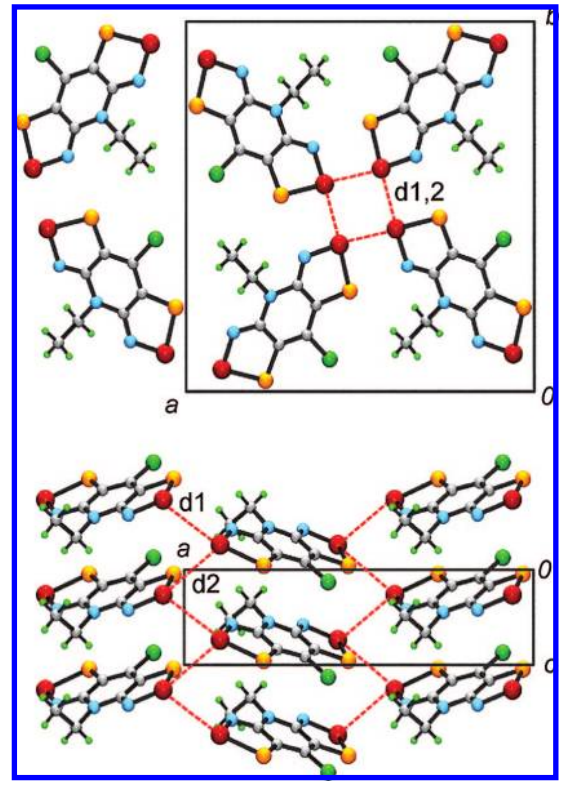

Figure 2. Unit cell drawings of **2a**, showing intermolecular Se---Se′ contacts *d*1 and *d*2.

(32) Bondi, A. *J. Phys. Chem.* **1964**, *68*, 441.

Table 2. Crystallographic Data and Metrics

formula	**2a**[a] $C_7H_5ClN_3S_2Se_2$	**2b** $C_8H_7ClN_3S_2Se_2$	**2c** $C_7H_2ClF_3N_3S_2Se_2$	**2d** $C_8H_8N_3S_2Se_2$	**2e** $C_7H_5CBrN_3S_2Se_2$
M	388.64	402.67	442.61	368.22	433.09
a (Å)	16.0334(8)	16.2209(8)	16.2612(8)	16.0088(17)	16.0885(7)
b (Å)	16.0334(8)	16.2209(8)	16.2612(8)	16.0088(17)	16.0885(7)
c (Å)	4.1090(4)	4.3831(4)	4.3882(4)	4.1385(9)	4.1339(3)
V (Å^3)	1056.30(13)	1153.27(13)	1160.36(13)	1060.60(30)	1070.02(10)
ρ_{calcd} (g cm^{-1})	2.444	2.319	2.534	2.306	2.688
space group	$P\bar{4}2_1m$	$P\bar{4}2_1m$	$P\bar{4}2_1m$	$P\bar{4}2_1m$	$P\bar{4}2_1m$
Z	4	4	4	4	4
temp (K)	296(2)	296(2)	296(2)	296(2)	296(2)
μ (mm^{-1})	7.61	6.98	6.98	7.33	11.00
λ (Å)	0.71073	0.71073	0.71073	0.71073	0.71073
data/restr./parameters	1150/0/76	1263/0/82	1296/12/91	1161/5/81	1166/0/76
solution method	direct methods	direct methods	direct methods	direct methods	direct methods
R, R_w (on F^2)	0.0447, 0.1003	0.0230, 0.0482	0.0234, 0.0609	0.0337, 0.0793	0.0173, 0.0402
Se1−S1 (Å)	2.249(2)	2.243(1)	2.233(1)	2.233(1)	2.244(1)
Se1−N1 (Å)	1.805(6)	1.823(3)	1.824(4)	1.814(4)	1.820(3)
C2−S1 (Å)	1.733(7)	1.735(3)	1.736(4)	1.735(5)	1.740(3)
$d1$ (Å)	3.328(1)	3.490(1)	3.407(1)	3.343(1)	3.344(1)
$d2$ (Å)	3.459(1)	3.554(1)	3.630(1)	3.470(1)	3.490(1)
$d3$ (Å)	3.818(1)	3.899(1)	3.885(1)	3.825(1)	3.845(1)
δ (Å)[b]	3.516(7)	3.501(3)	3.544(5)	3.508(5)	3.517(3)
τ (deg)[c]	58.83(1)	50.00(1)	53.86(1)	57.95(1)	58.29(1)
deviation from plane (Å)	0.087	0.075	0.0563	0.0891	0.093

[a] Data from ref.[28] [b] Separation of the mean molecular planes along the π-stacks. [c] Angle between the mean molecular planes and the stacking axis.

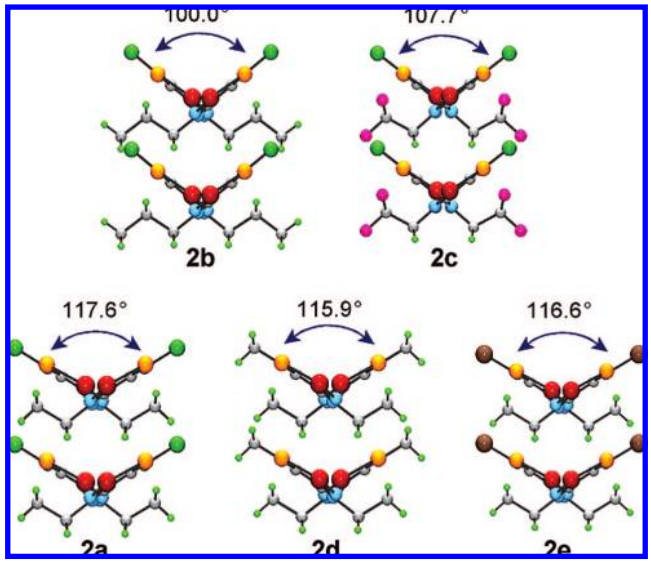

Figure 3. Cross-braced π-stacks, viewed parallel to {1,1,0}, showing the "butterfly wing" angle (2τ) between molecular planes.

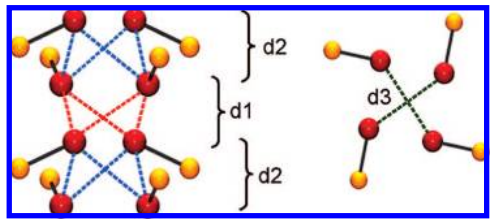

Figure 4. Stacked centers along z, viewed from the side (left) and top (right), with Se---Se′ contacts $d1$, $d2$, and $d3$.

on electronic and magnetic properties is unlikely to be large, a conclusion confirmed by the DFT calculations described below.

Band Structure Calculations. In order to compare the extent of intermolecular electronic interactions in the five radicals **2a**−**e**, in particular the consequences of the presence of the slightly larger R_1 groups in **2b** and **2c**, we have performed extended Hückel theory (EHT) band structure calculations on all five crystal structures (using the ambient temperature coordinates). The results should be viewed with caution, as in strongly correlated systems such as these the tight-binding model fails to provide a proper description of the ground state. These failings notwithstanding, the EHT method can, within a closely related series of structures, provide qualitative insight into trends in orbital interactions, and hence bandwidth W, which in this case we estimated in terms of the energetic spread (dispersion) of the four crystal orbitals (COs) arising from the interaction of the four SOMOs in the unit cell. The results are illustrated in Figure 5, which shows the four frontier COs plotted along the reciprocal space direction Γ (0,0,0) to Z (0,0,$^1/_2$). By virtue of the tetragonal symmetry, CO trends along this reciprocal space vector can be associated precisely with orbital interactions along the stacking axis in real space. The tetragonal symmetry also leads to the degeneracy (coincidence) of two of the COs,

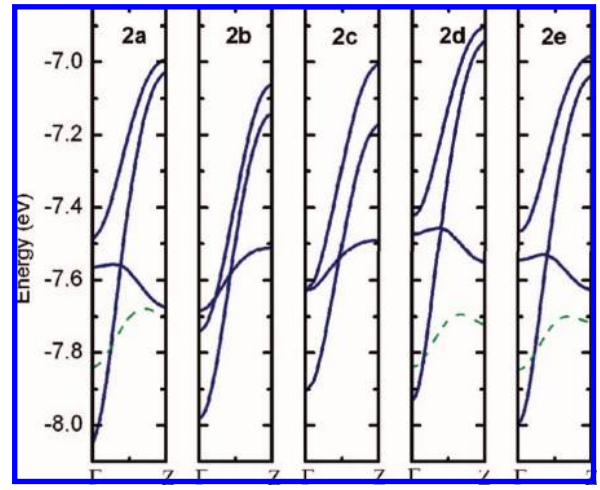

Figure 5. CO dispersion curves from Γ (0,0,0) to Z (0,0,$^1/_2$). Dashed lines are intruder bands.

Table 3. Bandwidth, Conductivity, and Magnetic Parameters

	2a[a]	2b	2c	2d	2e
W (eV)	1.06	0.90	0.90	1.03	1.01
σ(300 K) (S cm^{-1})	1.0×10^{-4}	5.0×10^{-5}	1.8×10^{-5}	1.9×10^{-4}	1.2×10^{-4}
E_{act} (eV)	0.27	0.31	0.31	0.27	0.29
C (emu K mol^{-1})	0.369	0.383	0.373	0.391	0.394
θ (K)	20.3	−3.5	−0.4	18.4	21.0
T_c (K)	12.8	---	---	13.6	14.1
M_{sat} (Nβ) at 2 K	1.00	---	---	0.98	1.02
M_{rem} (Nβ) at 2 K	0.41	---	---	0.38	0.42
H_c (Oe) at 2 K	250	---	---	230	320

[a] Data from ref 28b.

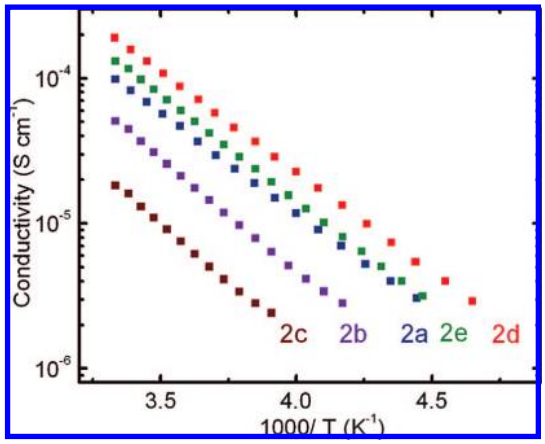

Figure 6. Log σ versus $1/T$ plots for **2a**−**e**. Derived activation energies are in Table 3.

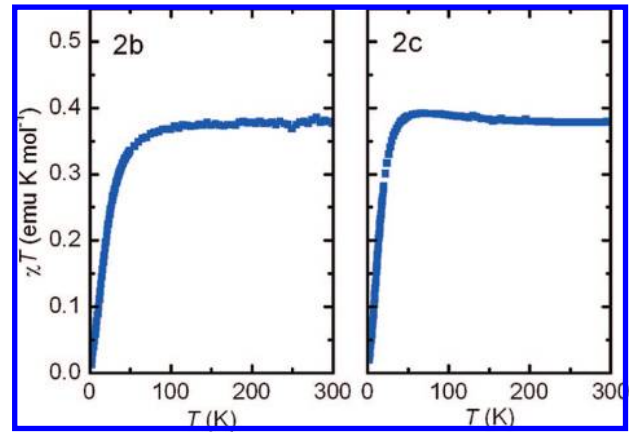

Figure 7. Plots of χT (field-cooled) versus temperature at $H = 1000$ Oe for **2b** and **2c**.

and in the case of **2a**, **2d**, and **2e** there is an intruder orbital[33] that falls in the same energy range.

Overall, the appearance of the dispersion curves is much the same. The bandwidth W (Table 3) of all five compounds is near 1 eV, a remarkably large value for a molecular compound, but in keeping with the tight crystal packing. Closer inspection, however, reveals some subtle differences. From the spread of the dispersion curves across the series, it is apparent that W for compounds **2b** and **2c** is less than for the other three compounds. This conclusion is consistent with the longer intermolecular contacts observed for these two radicals. Their electronic structures are also slightly more one-dimensional.

Conductivity and Magnetic Measurements. The results of the band structure calculations described above led us to believe that the conductivity characteristics of the five radicals **2a**−**e** would be similar. The results of four-probe variable-temperature measurements, presented in Figure 6 in the form of plots of log σ versus $1/T$, confirm these expectations. Despite the high EHT bandwidths found for these systems, they are not metals; their conductivity remains activated, with σ(300 K) spanning a range from 10^{-5} to 10^{-4} S cm^{-1}. Within the series, however, the slightly lower conductivities and higher activation energies E_{act} for **2b** and **2c** (Table 3) are in accord with the reduced bandwidths estimated for these two radicals.

Magnetic susceptibility measurements have been performed on **2a**−**e** over the temperature range 2−300 K. Above 50 K, the static susceptibility χ (corrected for diamagnetic contributions) of all five compounds is that expected for an $S = {}^1/_2$ paramagnet; values of C and θ derived from Curie−Weiss fits to the high-temperature data are listed in Table 3. Below 50 K, the behavior within the series diverges, and for both presentation and discussion purposes it is convenient to separate the results for the new compounds **2b**−**e** into two groups: (i) those with a common basal substituent (R_2 = Cl), that is, **2b** and **2c**, and (ii) those with a common *N*-alkyl group (R_1 = Et), that is, **2d** and **2e**.

The effect of replacement of the ethyl group in **2a** by a propyl (**2b**) or trifluoroethyl (**2c**) substituent is dramatic. The phase transition to a ferromagnetically ordered state observed for **2a** is completely lost in the two more sterically encumbered variants. Plots of χT versus T at $H = 1000$ Oe (Figure 7) are consistent with Curie−Weiss behavior, with the value of χT holding steady over the range 300−50 K near 0.375 emu K mol^{-1}, as expected for an $S = {}^1/_2$ paramagnet with a g-value nominally equal to 2.[34] Below 50 K, the value of χT drops sharply, indicative of the onset of weak antiferromagnetic exchange interactions. There was no indication, based on ZFC-FC experiments, of magnetic ordering (AFM or canted AFM) in either of these two radicals.

In contrast to compounds **2b** and **2c**, where ferromagnetic ordering is not observed, radicals **2d** and **2e** behave in a manner very similar to the parent radical **2a**. Both show large, positive (ferromagnetic) Weiss constants (Table 3), with values of χT(300 K) of 0.417 and 0.422 emu K mol^{-1} for **2d** and **2e**, respectively, and plots of χT (field-cooled) versus T at $H = 100$ Oe reveal the same low-temperature ferromagnetic surge seen for **2a**. As shown in Figure 8, χT starts to rise rapidly just below 20 K and reaches maximum values of 183 emu K mol^{-1} at 10 K for **2d** and 214 emu K mol^{-1} at 11 K for **2e**.

(33) An intruder orbital is a crystal orbital from a lower lying band that overlaps with the four dispersion curves being examined.

(34) The g-value for **2a** (from EPR measurements) is 2.0111. See ref 28.

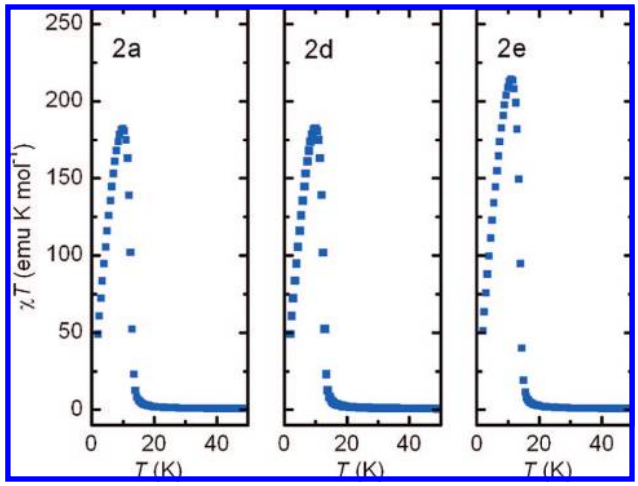

Figure 8. Plots of χT (field-cooled) versus temperature at $H = 100$ Oe for **2a**, **2d**, and **2e**.

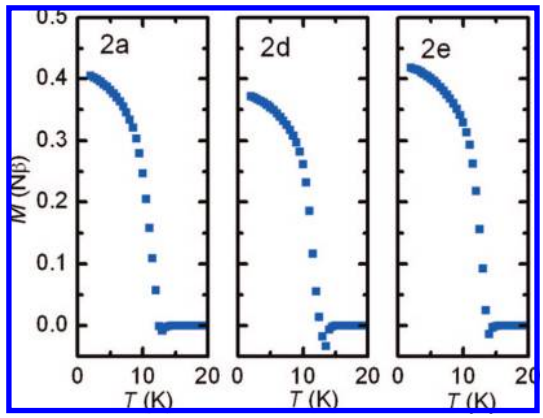

Figure 9. Field-independent magnetization as a function of temperature for **2a**, **2d**, and **2e**.

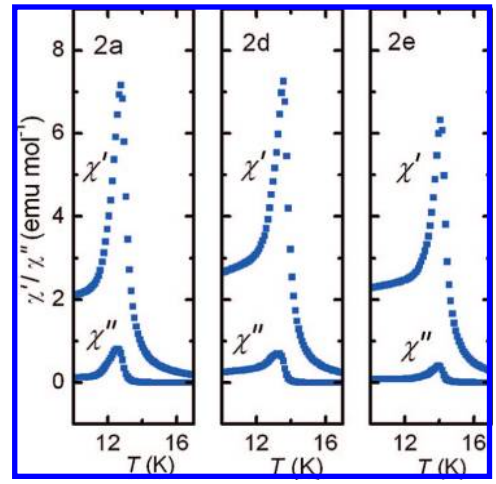

Figure 10. In-phase χ' and out-of-phase χ'' AC magnetic susceptibility (at 1 kHz) of **2a**, **2d**, and **2e** as a function of temperature.

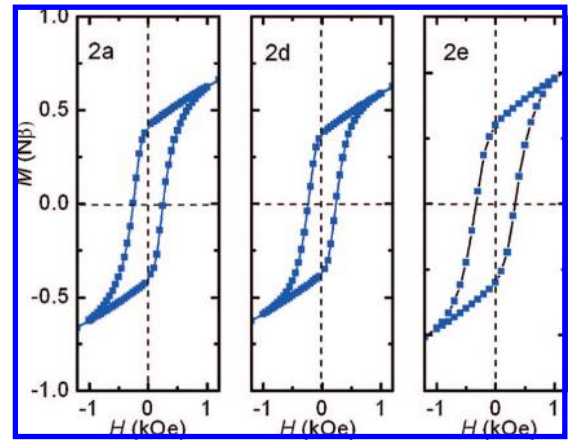

Figure 11. Magnetization of **2a**, **2d**, and **2e** as a function of magnetic field at 2 K.

Measurements of the field-independent magnetization M_{sp} of **2d** and **2e** provided additional evidence for the existence of ferromagnetically ordered states, as found for **2a**, and also afforded a qualitative measure of the ordering temperatures. As illustrated in Figure 9, M_{sp} decays rapidly with temperature, as thermal energy overcomes magnetic ordering, reaching a value of zero near 12.5 (**2a**), 13.5 (**2d**), or 14.0 K (**2e**), in accord with the point of maximum slope in the χT versus T plots described above. Back-extrapolation to $T = 0$ K afforded values of M_{sp}, the spontaneous magnetization at 0 K, near 0.39 (**2d**) and 0.41 Nβ (**2e**). Variable AC susceptibility measurements at different frequencies allowed us to pinpoint the ordering temperatures T_c of the two compounds. As shown in Figure 10, **2d** and **2e** both show sharp, well-defined maxima in the real (in-phase, χ') and imaginary (out-of-phase, χ'') components at 13.6 and 14.1 K respectively. Both values are slightly higher than that found for **2a** (12.8 K), and, as in the case for **2a**, the invariance of T_c with changes in the cycling frequency (from 50 Hz to 5 kHz) confirms that the materials are not spin glasses.

We also performed magnetization experiments as a function of field on **2d** and **2e**. In both cases M rises sharply with H, reaching (at 2 K) a maximum at $H = 10$ kOe, after which there is no further change in M with H (up to 55 kOe). The corresponding saturation magnetization values M_{sat} are 0.98 Nβ for **2d** and 1.02 Nβ for **2e**, in good agreement with that expected ($M_{sat} = g$N$\beta S = 1$ Nβ) for an $S = {}^1/_2$ system with $g = 2$. As in the case of **2a**, reversal and cycling of the field sweep leads to hysteresis in the magnetization for both **2d** and **2e**. Plots of M versus H for all three compounds, from measurements taken at 2 K, are shown in Figure 11. The remanent magnetization M_{rem} of the three compounds is virtually the same, and the coercive field H_c (at 2 K) varies from 230 Oe in **2d** to 250 Oe in **2a** and 320 Oe in **2e**.

Magnetic Exchange Interactions. The crystal structures of the five radicals reported here show subtle but important differences in packing. The larger size of the propyl and trifluoroethyl groups leads to an increase in plate slippage for **2b**,**c** (a decrease in τ), a concomitant increase in the unit cell repeat distance c, and a separation of the radicals about the $\bar{4}$ points. Collectively these adjustments lead to predictable decreases in electronic bandwidth and a slight reduction in conductivity for **2b**,**c**. However, these changes, like the packing differences that caused them, are incremental. By contrast, the difference in the magnetic response of the five radicals is dramatic. Three radicals (**2a**,**d**,**e**) show clear and impressive signatures for a phase transition to a ferromagnetically ordered state with an ordering temperature T_c in the range 13−14 K, while the other two (**2b**,**c**) show no indication of magnetic ordering, be it ferromagnetic or antiferromagnetic, at any temperature down to 2 K. This dichotomy is striking and raises several questions. What is the origin of this sharp difference in magnetic behavior? How and

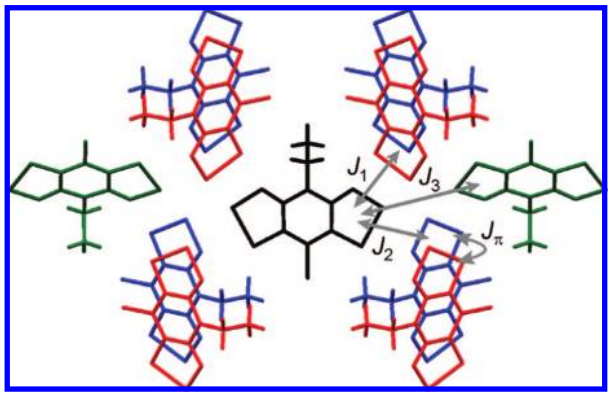

Figure 12. Pairwise exchange interactions J_1, J_2, J_3, and J_π in **2a**.

why do the seemingly minor changes in packing lead to a "switching off" of magnetic ordering in **2b** and **2c**?

In order to address these questions, we have undertaken an analysis of the direct through-space magnetic interactions in the structures of **2a**−**e**. In this so-called first principles approach,[35] the bulk magnetic properties of a crystalline radical are represented as a composite of the individual exchange interactions arising from all pairwise combinations of each radical and its nearest neighbors in the lattice. The method, which has been successfully applied to a variety of nitrogen-centered radicals,[36] heterocyclic thiazyls,[37,38] and phenalenyls,[39] employs exchange energies estimated from broken-symmetry DFT methods developed by Noodleman.[40] Accordingly, and with reference to the Heisenberg Hamiltonian $H_{ex} = -2J\{S_1 \cdot S_2\}$, the exchange energy J for any pair of interacting radicals can be estimated from the total energies of the triplet (E_{TS}) and broken-symmetry singlet (E_{BSS}) states and the respective expectation values $\langle S^2 \rangle$ of the two states according to eq 1.

$$J = \frac{-(E_{TS} - E_{BSS})}{\langle S^2 \rangle_{TS} - \langle S^2 \rangle_{BSS}} \quad (1)$$

The calculation of exchange energies was restricted to simple dinuclear exchange between nearest neighbors. In addition to the exchange energy associated with interactions between radicals within the π-stacks, which we denote as J_π, there is a total of eight pairwise interactions possible between each radical and those in nearest neighbor π-stacks; these are illustrated in Figure 12 using radical **2a** as an example. Fortunately, the high symmetry of the lattice is such that the eight interactions fall into two groups characterized by the Se---Se′ separations $d1$ and $d2$ noted earlier (see Figures 2 and 4); we define the associated exchange energies as J_1 and J_2, respectively. Finally, there are two head-to-head interactions J_3 arising from the second nearest neighbor π-stack contacts $d3$ across the $\bar{4}$ centers (Figure 4). For each of the four unique interactions, that is, J_1, J_2, J_3, and J_π, single-point total energies E_{TS} and E_{BSS} were calculated using the hybrid exchange correlation functional UB3LYP and polarized, split-valence basis sets with double-zeta (6-31G(d,p)) and triple-zeta (6-311G(d,p)) functions. Atomic coordinates were taken from the 100 K data sets on each of the radicals.

Table 4. UB3LYP/6-311G(d,p) Exchange Energies[a]

	J_1	J_2	J_3	J_π
2a	7.15	0.26	−0.48	−1.29
2b	5.25	4.59	0.50	−30.24
2c	6.65	4.10	0.20	−23.53
2d	6.65	0.77	−0.22	−3.63
2e	6.67	0.61	−0.50	−3.89

[a] In cm^{-1}, from single-point calculations using eq 1. Interactions J_1, J_2, J_3, and J_π are defined in Figure 12.

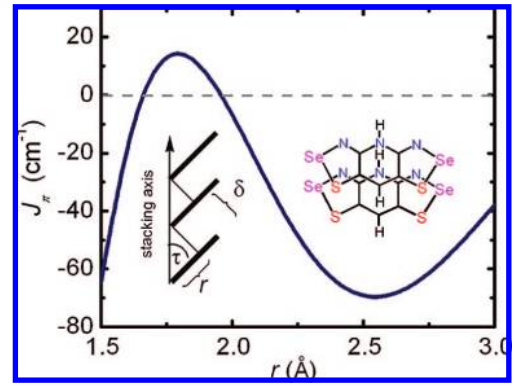

Figure 13. UB3LYP/6-31G(d,p) exchange energy J_π as a function of r for **2** ($R_1 = R_2 = H$), with $\delta = 3.45$ Å.

The numerical results from these single-point calculations (Table 4) prompt several observations. First, there is a marked variation in J_π within the series. While radicals **2a**,**d**,**e** (the ferromagnetic set) display negative J_π-values, they are relatively close to zero and the ferromagnetic domain. By contrast, the large negative values for **2b**,**c** are an unequivocal indication of strong antiferromagnetic exchange. Second, the interstack exchange energy J_1 is largely independent of variations in $d1$. Moreover, its relatively large positive value across the entire series heralds a ferromagnetic interaction. The other lateral exchange term J_2 is also ferromagnetic, although its magnitude is less; somewhat surprisingly, the least positive values are those found for **2a**,**d**,**e**. Finally, the magnitude of J_3 is near zero in all cases, as expected from the large separation $d3$. This latter interaction is unlikely to play a major role in determining magnetic properties.

Given the marked differences in the values of J_π found in **2b**,**c** versus **2a**,**d**,**e**, we carried out a second series of calculations, this time at the UB3LYP/6-31G(d,p) level, using an idealized pair of prototypal radicals **2** ($R_1 = R_2 = H$). The purpose of this analysis was to establish a clearer view of the dependency of J_π on π-stack slippage. In these model calculations, the degree of slippage was driven by means of changes in the translational coordinate r, defined in Figure 13, which can be related to the inclination angle τ and the plate-to-plate separation δ (Table 2) by the expression $\tau = \tan^{-1}(\delta/r)$. The value of δ was set at 3.45 Å, which is close to the average (3.44 Å) of the values

(35) Deumal, M.; Robb, M. A.; Novoa, J. J. *Prog. Theor. Chem. Phys.* **2007**, *16*, 271.
(36) (a) Novoa, J. J.; Deumal, M. *Struct. Bonding (Berlin)* **2001**, *100*, 33. (b) Jornet, J.; Deumal, M.; Ribas-Ariño, J.; Bearpark, M. J.; Robb, M. A.; Hicks, R. G.; Novoa, J. J. *Chem. Eur. J.* **2006**, *12*, 3995.
(37) (a) Rawson, J. M.; Luzon, J.; Palacio, F. *Coord. Chem. Rev.* **2005**, *249*, 2631. (b) Luzon, J.; Campo, J.; Palacio, F.; McIntyre, G. J.; Rawson, J. M. *Polyhedron* **2005**, *24*, 2579. (c) Deumal, M.; LeRoux, S.; Rawson, J. M.; Robb, M. A.; Novoa, J. J. *Polyhedron* **2007**, *26*, 1949.
(38) (a) Decken, A.; Mattar, S. M.; Passmore, J.; Shuvaev, K. V.; Thompson, L. K. *Inorg. Chem.* **2006**, *45*, 3878. (b) Leitch, A. A.; Oakley, R. T.; Reed, R. W.; Thompson, L. K. *Inorg. Chem.* **2007**, *46*, 6261.
(39) Takano, Y.; Taniguchi, T.; Isobe, H.; Kubo, T.; Morita, Y.; Yamamoto, K.; Nakasuji, K.; Takui, T.; Yamaguchi, K. *J. Am. Chem. Soc.* **2002**, *124*, 11122.
(40) (a) Noodleman, L.; Norman, J. G. *J. Chem. Phys.* **1979**, *70*, 4903. (b) Noodleman, L. *J. Chem. Phys.* **1981**, *74*, 5737.

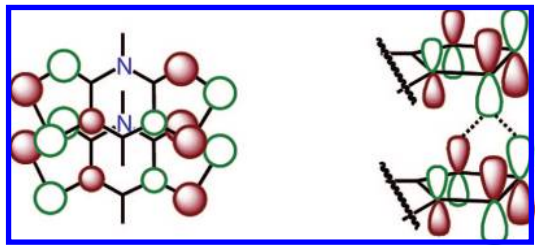

Figure 14. Orthogonal overlap of adjacent SOMOs along slipped π-stacks of **2a**,**d**,**e**.

found for the five radicals at 100 K, and the resulting exchange energies are plotted as a function of r in Figure 13.

The model $J_\pi(r)$ calculations indicate that, for very small degrees of slippage ($r < 1.7$ Å or $\tau > 64°$), as the radicals move toward direct superposition, J_π becomes large and negative, heralding the onset of a singlet state. At larger degrees of slippage, that is, $r > 2.0$ Å (or $\tau < 60°$), the value of J_π turns strongly negative and remains so to the limit of the calculations ($r = 3.0$ Å or $\tau = 49°$). However, between these two deep antiferromagnetic "trenches" there is a small ferromagnetic "island" (1.7 Å $< r <$ 2.0 Å) where J_π is positive. Comparison of these computed results with the observed structures is revealing. Radicals **2a**,**d**,**e** all cluster near $r = 2.1$ Å, that is, just outside the nominal ferromagnetic zone, while **2b** ($r = 2.62$ Å) and **2c** ($r = 2.51$ Å) both lie well inside the strongly antiferromagnetic region.

Taken together, the single-point and model plate slippage calculations allow for a qualitative interpretation of the differences in the magnetic behavior observed in the five radicals under study. While the results do not predict the onset of ferromagnetic ordering in **2a**,**d**,**e**, they do indicate that local pairwise interactions within and between the π-stacks in these radicals are all ferromagnetic or nearly so. The slightly negative J_π values may simply reflect the coarseness of the model and/or the inadequacy of the computational method. Either way, the cumulative effect of the multiple ferromagnetic interactions J_1 and, to a lesser extent, J_2 lateral to the π-stacks may well be sufficient to compensate for any weak antiferromagnetic terms along the stacking direction. By contrast, the much stronger antiferromagnetic J_π values predicted for **2b**,**c** are too large to be offset by the positive J_1 and J_2 exchange energies that these radicals possess. As a result, ferromagnetic ordering for **2b**,**c** is not expected. In more general terms, the variations in J_π as a function of plate slippage (r) reveal that there is, at best, an alarmingly small range of r-values (1.7 Å $< r <$ 2.0 Å) associated with ferromagnetic exchange energies. In this light, the isolation of three radicals **2a**,**d**,**e** with degrees of slippage close to this ferromagnetic "island" is nothing if not fortunate. Likewise, the paramagnetic materials **2b**,**c** probably represent the rule rather than the exception for these radicals in the $P\bar{4}2_1m$ space group.

Finally, and in order to place the through-space model in an orbital context, it is instructive to examine the nature of the intermolecular SOMO−SOMO overlaps along the π-stacks, with a view to assessing their impact on the degree of ferromagnetic or antiferromagnetic coupling. The spin distributions in the present radicals are, however, highly delocalized and the intermolecular interactions numerous. Some qualitative conclusions can, nonetheless, be drawn. As illustrated in Figure 14, the a_2 SOMO in **2** is strongly antibonding,[22b] and in the slipped π-stacked arrays prescribed by the tetragonal space group, the overlap between SOMOs on neighboring radicals along the stack is dominated by the interaction between a pπ-orbital on sulfur in one ring with the pπ-orbital on nitrogen and selenium on its neighbor. The effect of this alignment on reducing bandwidth (by nullifying overlap) in bisdithiazolyls was recognized some time ago,[17b] but within the present context it provides a classic example of the magnetically orthogonal overlap required to promote ferromagnetic exchange.[41] In terms of this model, the SOMO−SOMO overlap in **2a**,**d**,**e** can be viewed as being close to perfectly orthogonal, but with increasing slippage, as in **2b**,**c**, overlap and antiferromagnetic exchange interactions increase.

Summary and Conclusion

For decades synthetic chemists have pursued the idea of using organic radicals as carriers of charge or spin.[42] Recent findings[28] of ferromaganetic heavy-atom heterocyclic radicals with $T_c > 10$ K, coercivities $H_c > 1000$ Oe (at 2 K), and conductivities $\sigma_{RT} > 10^{-4}$ S cm^{-1} have provided strong evidence that multifunctional materials, that is, radicals exhibiting both conductive and magnetic properties, can be made. The challenge for the future is not only to improve the performance of these systems but also to learn more about the structural factors that give rise to their remarkable properties. In the present work we have carried out a systematic study of the solid-state structures and transport properties of the series of tetragonal (space group $P\bar{4}2_1m$) bis(thiaselenazyl) radicals **2a**−**e**. We have found that minor changes in packing occasioned by the differing steric requirements of the *N*-alkyl substituent R_1 give rise to major changes in magnetic properties. Radicals **2a**,**d**,**e** order ferromagnetically with T_c's of 13−14 K, while **2b**,**c** behave as Curie−Weiss paramagnets down to 2 K. Using broken-symmetry DFT methods to estimate nearest neighbor radical−radical exchange energies, we have found that magnetic exchange interactions along the radical π-stacks are acutely sensitive to the degree of slippage of the stacks. Favorable (ferromagnetic) exchange energies are only found over a narrow window of inclination angles. The slipped π-stacks in **2b**,**c** fall well outside this window, while those of **2a**,**d**,**e** are close to if not inside it. Ongoing synthetic efforts aimed at increasing the ordering temperature are focused on varying the building blocks through careful choice of R_1 and R_2 substituents in order to modify *slightly* the π-stack slippage found for **2a**,**d**,**e**.

Experimental Section

General Procedures and Starting Materials. The reagents selenium dioxide, trifluoroethyl triflate, ethyl triflate, propyl triflate, ammonia gas, sulfur monochloride, bromine, tetra-*n*-butylammonium bromide, silver triflate, octamethylferrocene (OMFc), decamethylferrocene (DMFc), and *N*,*N*,*N*′,*N*′-tetramethyl-*p*-phenylenediamine (TMPDA) were obtained commercially. 2,6-Dichloro-4-methylpyridine, [**1a**,**b**][OTf], [**1**][$GaCl_4$] (R_1 = Et; R_2 = H), **5**,[17] [**2a**][OTf], and **2a**[28] were prepared according to literature methods. OMFc and DMFc were purified by sublimation in vacuo and recrystallization from acetonitrile, and TMPDA was purified by sublimation in vacuo. The solvents acetonitrile (MeCN), dichloroethane (DCE), acetic acid (HOAc), diethyl ether, ethyl acetate, and dichloromethane (DCM) were of at least reagent grade. MeCN was dried by distillation from P_2O_5 and/or CaH_2, and both DCE

(41) (a) Kahn, O. *Molecular Magnetism*; VCH: New York, 1993. (b) Kahn, O.; Galy, J.; Journaux, Y.; Jaud, J.; Morgenstern-Badarau, I. *J. Am. Chem. Soc.* **1982**, *104*, 2165. (c) Verdaguer, M. *Polyhedron* **2001**, *20*, 1115.
(42) Day, P. *Nature* **1993**, *363*, 113.

and DCM were dried by distillation from P_2O_5. All reactions were performed under an atmosphere of dry nitrogen. Melting points are uncorrected. Infrared spectra (Nujol mulls, KBr optics) were recorded on a Nicolet Avatar FTIR spectrometer at 2 cm^{-1} resolution. ^1H spectra were run on a Bruker Avance 300 MHz NMR spectrometer, and low-resolution ESI mass spectra were run on a Micromass Q-TOF Ultima Global LC/MS/MS system. Elemental analyses were performed by MHW Laboratories (Phoenix, AZ).

Preparation of 8-Chloro-4-trifluoroethyl-4*H*-bis[1,2,3]dithiazolo[4,5-*b*:5′,4′-*e*]pyridin-2-ium Triflate, [1c][OTf]. Neat 2,2,2-trifluoroethyl triflate (3.5 mL, 24.0 mmol) was added to a stirred slurry of **5** (2.38 g, 8.95 mmol) in 25 mL of DCE in a small glass pressure vessel. The vessel was sealed, and the mixture was heated in an oil bath at 100 °C for 40 h. The reaction mixture was cooled to room temperature, and crude [**1c**][OTf], a dark red solid, was filtered off, washed with 5 × 20 mL of DCE, and dried in air; yield, 3.63 g (7.29 mmol, 81%). Recrystallization from MeCN afforded copper-colored plates, dec >300 °C. IR: 1520 (w), 1497 (s), 1438 (s), 1365 (s), 1274 (s), 1240 (vs), 1169 (s), 1108 (m), 1027 (s), 1008 (w), 931 (w), 866 (w), 841 (w), 831 (w), 767 (vs), 716 (w), 689 (w), 676 (w), 669 (s), 640 (s), 574 (w), 539 (w), 516 (m), 479 (s) cm^{-1}. Anal. Calcd for $C_8H_2ClF_6N_3O_3S_5$: C, 19.30; H, 0.40; N, 8.44. Found: C, 19.55; H, 0.41; N, 8.67.

Preparation of *N*-Ethyl-2,6-diamino-4-methylpyridinium Triflate, [6][OTf]. Ethyl triflate (8.04 mL, 0.0622 mol) was added to a colorless solution of 2,6-dichloro-4-methylpyridine (8.40 g, 0.0518 mol) in 20 mL of DCE, and the reaction mixture was stirred for 16 h to afford a heavy white precipitate, to which 40 mL of diethyl ether was added. After 5 min, the mixture was cooled to −20 °C for 1 h and then filtered on a fine (E porosity) glass frit. The resulting white solid was washed with 2 × 30 mL of cold diethyl ether and dried in vacuo. Recrystallization from a 3:1 solution of ethyl acetate/DCE afforded white needles of *N*-ethyl-2,6-dichloro-4-methylpyridinium triflate; yield, 11.2 g (0.0329 mol, 64%); mp, 146−147 °C. IR: 3070 (w), 1615 (s), 1264 (vs), 1245 (s), 1227 (m), 1159 (m), 1144 (s), 1034 (s), 841 (w), 640 (s), 517 (w) cm^{-1}. ^1H NMR (δ, CD_3CN): 7.92 (s, 2H), 4.86 (q, 2H, J = 7.25 Hz), 2.55 (s, 3H), 1.51 (t, 3H, J = 7.25 Hz). Anal. Calcd for $C_9H_{10}Cl_2F_3NO_3S$: C, 31.78; H, 2.96; N, 4.12. Found: C, 31.88; H, 3.10; N, 3.96. Ammonia gas was bubbled through an ice-cold mixture of *N*-ethyl-2,6-dichloro-4-methylpyridinium triflate (9.27 g, 0.0273 mol) in 150 mL of MeCN in a large glass pressure vessel. The vessel was then sealed and heated at 80 °C for 18 h. After the mixture was cooled to room temperature and the reaction vessel vented, the mixture was heated at 90 °C for 3 h to release excess ammonia. The yellow solid was removed by filtration on a Büchner funnel, and the solvent from the filtrate was evaporated to give the thick orange oil of [**6**][OTf], which was used in the next step without purification; yield, 8.23 g (0.0273 mol, 100%). ^1H NMR (δ, CD_3CN): 6.02 (s, 2H), 3.91 (q, 2H, J = 7.37 Hz), 2.15 (s, 3H), 1.30 (t, 3H, J = 7.37 Hz).

Preparation of 8-Methyl-4-ethyl-4*H*-bis[1,2,3]dithiazolo[4,5-*b*:5′,4′-*e*]pyridin-2-ium Triflate [1d][OTf]. Sulfur monochloride (6.55 mL, 0.0818 mol) was added to a solution of [**6**][OTf] (7.49 g, 0.0249 mol) in 45 mL of a 2:1 solution of DCE/MeCN. The initially green solution was heated at a gentle reflux for 5 h, and the resulting blue solution was then cooled to room temperature. The mixture was further cooled to −20 °C for 1 h before the red microcrystalline precipitate of crude [**1d**][OTf] was collected on a fine (E porosity) glass frit, washed with 2 × 40 mL of DCM, and dried in vacuo; yield, 6.67 g (0.0157 mol, 64%). The crude material was further washed with 75 mL of CS_2 and 150 mL of hot DCE before being recrystallized from 100 mL of MeCN to give [**1d**][OTf] as red needles; yield, 3.76 g (56% from crude); mp, 228 °C. IR: 1366 (s), 1279 (m), 1251 (m), 1224 (w), 1159 (w), 1031 (m), 740 (m), 638 (m) cm^{-1}. Anal. Calcd for $C_9H_8F_3N_3O_3S_5$: C, 25.52; H, 1.90; N, 9.92. Found: C, 25.50; H, 1.81; N, 9.79.

Preparation of 8-Bromo-4-ethyl-4*H*-bis[1,2,3]dithiazolo[4,5-*b*:5′,4′-*e*]pyridin-2-ium Triflate [1e][OTf]. A solution of bromine (0.92 mL, 17.9 mmol) in 7 mL of MeCN was added to a solution of [**1**][$GaCl_4$] (4.24 g, 8.98 mmol) in 250 mL of MeCN, and the reaction mixture was heated at reflux. After 1 h, tetra-*n*-butylammonium bromide (3.23 g, 10.0 mmol) was added, to give a green precipitate that was warmed at about 60 °C for 30 min and then cooled to room temperature. The green solid of [**1e**][Br] was filtered and washed with 3 × 100 mL of MeCN; yield, 3.76 g (8.97 mmol, 100%). IR: 1505 (w), 1482 (m), 1449 (s), 1428 (m), 1354 (s), 1187 (w), 1181 (w), 1005 (w), 887 (w), 796 (m), 759 (s), 713 (w), 665 (w), 558 (w), 535 (w), 528 (w), 478 (w) cm^{-1}. Silver triflate (2.86 g, 11.1 mmol) was added to a slurry of [**1e**][Br] (3.76 g, 8.97 mmol) in 200 mL of MeCN to give a blue solution that was heated at about 60 °C for 45 min before being filtered hot through paper to remove some of the silver bromide. The filtrate was concentrated to 75 mL, and upon standing for 16 h, the red solid of [**1e**][OTf] crystallized. The solid was filtered and washed with 40 mL of DCM; yield, 2.30 g (4.71 mmol, 52%). Crude product was recrystallized from MeCN and isolated as red needles, dec >280 °C. IR: 1515 (m), 1486 (s), 1434 (s), 1356 (s), 1271 (s), 1242 (s), 1227 (s), 1189 (m), 1168 (m), 1182 (m), 1126 (s), 1007 (w), 889 (w), 878 (w), 803 (m), 792 (m), 758 (s), 669 (s), 638 (s), 592 (w), 574 (w), 544 (w), 515 (m), 475 (s) cm^{-1}. Anal. Calcd for $C_8H_5BrF_3N_3O_3S_5$: C, 19.67; H, 1.03; N, 8.60. Found: C, 20.06; H, 0.75; N, 8.36.

Preparation of Bis[1,2,3]thiaselenazolo[4,5-*b*:5′,4′-*e*]pyridin-2-ium Triflates. [2b,c,e][OTf]. Compound [**1b**,**c**,**e**][OTf] (2.00 mmol) and finely ground selenium dioxide (0.666 g, 6.00 mmol) were added to a large glass pressure vessel along with 80 mL of MeCN, and the mixture was stirred and heated in an oil bath at 110 °C for 48−72 h. The reaction was continued until analysis of the mixture by ESI-MS showed complete and specific formation of $[\mathbf{2}]^+$. The flask was cooled to room temperature and the dark green solution filtered through a glass Büchner funnel to remove a small amount of black precipitate. The filtrate was concentrated to 30 mL and cooled to room temperature for 1 h, then at −20 °C for 2 h. Red crystals of [**2b**,**c**,**e**][OTf] were filtered off, washed with DCM, and dried in air. The product was double-recrystallized from MeCN and/or HOAc as red needles.

[2d][OTf]. Finely ground selenium dioxide (1.22 g, 11.0 mmol) was added to a hot blue solution of [**1d**][OTf] (1.55 g, 3.66 mmol) in 40 mL of HOAc. The mixture was heated at reflux for 70 min, after which the green solution was cooled to room temperature. The resulting red crystals of [**2d**][OTf] were filtered off and washed with 20 mL of HOAc and 20 mL of DCM. The product was recrystallized from 100 mL of MeCN to give red needles.

Analytical Data for Salts. [2b][OTf]. Yield, 64%; mp, 260−262 °C. IR: 2257 (w, MeCN), 1437 (s), 1288 (s), 1240 (s), 1218 (s), 1180 (w), 1155 (s), 1147 (s), 1082 (w), 1027 (s), 972 (w), 754 (w), 735 (w), 719 (w), 637 (s), 595 (m), 571 (w), 551 (w), 516 (w), 476 (w) cm^{-1}. Anal. Calcd for $C_9H_7ClF_3N_3O_3S_3Se_2$: C, 19.59; H, 1.28; N, 7.62. Found: C, 19.43; H, 1.10; N, 7.68.

[2c][OTf]. Yield, 70%; dec >300 °C. IR: 2253 (w, MeCN), 1483 (s), 1286 (s), 1261 (s), 1238 (s), 1220 (s), 1189 (w), 1171 (s), 1147 (s), 1094 (s), 1024 (s), 997 (m), 842 (w), 829 (m), 758 (m), 748 (s), 719 (s), 684 (m), 638 (s), 611 (m), 593 (m), 573 (w), 540 (w), 515 (w), 474 (w) cm^{-1}. Anal. Calcd for $C_8H_2ClF_6N_3O_3S_3Se_2$: C, 16.24; H, 0.34; N, 7.10. Found: C, 16.41; H, 0.72; N, 7.23.

[2d][OTf]. Yield, 52%; dec >234 °C. IR: 1277 (m), 1238 (s), 1174 (w), 1024 (m), 722 (m), 633 (m), 594 (w) cm^{-1}. Anal. Calcd for $C_9H_8F_3N_3O_3S_3Se_2$: C, 20.90; H, 1.56; N, 8.12. Found: C, 21.17; H, 1.51; N, 7.95.

[2e][OTf]. Yield, 60%; dec >259 °C. IR: 1505 (m), 1428 (s), 1358 (s), 1200 (s), 1183 (s), 1159 (s), 1085 (w), 1059 (s), 1004 (m), 908 (w), 853 (s), 738 (s), 589 (s), 537 (m), 475 (m) cm^{-1}. Anal. Calcd for $C_8H_5BrF_3N_3O_3S_3Se_2$: C, 16.50; H, 0.87; N, 7.22. Found: C, 16.30; H, 0.78; N, 7.14.

Preparation of Radicals 2b−e. Method 1: Bulk Material for Conductivity and Magnetic Measurements. Before use, all glassware was soaked overnight in dilute HNO_3, then washed with deionized water followed by distilled water, and finally oven-dried

at 100 °C overnight. Magnetic stirbars were glass-covered. Degassed solutions (three freeze−pump−thaw cycles) of reducing agent (0.571−1.01 mmol) (**b**,**d**, DMFc; **c**, OMFc; **e**, TMPDA) in 40−125 mL of MeCN and [**2b**−**e**][OTf] (0.429−0.580 mmol) in 90−150 mL of MeCN were combined, and after 30 m the gold-brown precipitate of **2b**−**e** was filtered off and washed with 4 × 20 mL of MeCN.

Method 2: Diffusion H-Cells for Single-Crystal Growth. Degassed solutions (three freeze−pump−thaw cycles) of reducing agent (0.056−0.085 mmol) (**b**,**c**,**d**, OMFc; **e**, HMFc) in 15 mL of MeCN and [**2b**−**e**][OTf] (0.038−0.054 mmol) in 15 mL of MeCN were allowed to diffuse together slowly at room temperature over a period of 16 h. The solvent was decanted to leave metallic green-black needles of **2b**−**e** suitable for X-ray work.

Analytical Data for Radicals. 2b. Yield, 89%; dec >120 °C. IR: 1410 (m), 1319 (s), 1296 (w), 1279 (m), 1223 (s), 1176 (w), 1075 (s), 965 (s), 906 (w), 890 (m), 815 (m), 730 (s), 696 (s), 615 (m), 577 (m), 534 (m), 502 (w), 460 (m) cm^{-1}. Anal. Calcd for $C_8H_7ClN_3S_2Se_2$: C, 23.86; H, 1.75; N, 10.44. Found: C, 24.00; H, 1.66; N, 10.68.

2c. Yield, 68%; dec >120 °C. IR: 1405 (m), 1322 (s), 1251 (s), 1228 (w), 1184 (s), 1165 (s), 1090 (s), 984 (m), 836 (m), 815 (w), 734 (m), 697 (s), 680 (w), 613 (m), 572 (w), 541 (w), 529 (w), 460 (w) cm^{-1}. Anal. Calcd for $C_7H_2ClF_3N_3S_2Se_2$: C, 19.00; H, 0.46; N, 9.46. Found: C, 19.25; H, 0.33; N, 9.68.

2d. Yield, 89%; dec >150 °C. IR: 1319 (m), 1233 (s), 1178 (w), 1085 (w), 1006 (w), 978 (w), 837 (m), 702 (s), 613 (s), 539 (w), 461 (w) cm^{-1}. Anal. Calcd for $C_8H_8N_3S_2Se_2$: C, 26.09; H, 2.19; N, 11.41. Found: C, 26.42; H, 2.48; 11.62.

2e. Yield, 93%; dec >120 °C. IR: 1442 (s), 1402 (w), 1352 (w), 1322 (m), 1230 (m), 1171 (w), 1085 (w), 1062 (w), 997 (w), 889 (w), 838 (m), 709 (w), 692 (m), 570 (w), 518 (w), 453 (w) cm^{-1}. Anal. Calcd for $C_7H_5BrN_3S_2Se_2$: C, 19.41; H, 1.16; N, 9.70. Found: C, 19.67; H, 1.36; N, 9.76.

Cyclic Voltammetry. Cyclic voltammetry was performed using a PINE bipotentiostat (model AFCClBP1) with scan rates of 50−100 mV s^{-1} on solutions (<10^{-3} M) of [**2a**−**e**][OTf] in oxygen-free MeCN (dried by distillation from CaH_2) containing 0.1 M tetra-*n*-butylammonium hexafluorophosphate. Potentials were scanned with respect to the quasi-reference electrode in a single-compartment cell fitted with Pt electrodes and referenced to the Fc/Fc^+ couple of ferrocene at 0.38 V vs SCE.[43] The $E_{pa} - E_{pc}$ separation of the reversible couples was within 10% of that of the Fc/Fc^+ couple.

X-ray Measurements. Needles of **2a**−**e** were glued to glass fibers with epoxy. X-ray data were collected using ω scans with a Bruker APEX I CCD detector on a D8 three-circle goniometer and Mo Kα (λ = 0.71073 Å) radiation. The data were scanned using Bruker's SMART program and integrated using Bruker's SAINT software.[44] The structures were solved by direct methods using SHELXS-90[45] and refined by least-squares methods on F^2 using SHELXL-97,[46] incorporated in the SHELXTL[47] suite of programs.

Magnetic Susceptibility Measurements. DC and AC magnetic susceptibility measurements were performed over the range 2−300 K on a Quantum Design MPMS SQUID magnetometer and on an Oxford Instruments MagLab EXA.

Conductivity Measurements. Temperature-dependent conductivity measurements were performed on pressed pellet samples using a four-probe method. A homemade device was used to measure the voltage drop under dynamic vacuum. Silver paint was used to apply the electrical contacts.

Band Structure Calculations. Band electronic structure calculations were performed with the EHMACC suite of programs[48] using the Coulomb parameters of Basch, Viste, and Gray[49] and quasi-split valence basis sets adapted from Clementi and Roetti.[50] For bromine, a single-zeta basis set was employed.[51] The off-diagonal elements of the Hamiltonian matrix were calculated with the standard weighting formula.[52] Atomic positions were taken from the ambient-temperature crystallographic data.

Exchange Energy Calculations. All calculations were performed using the UB3LYP functional with 6-31G(d,p) and 6-311G(d,p) basis sets, as contained in the Gaussian 03W suite of programs.[53] Exchange energies for interacting radicals were computed from eq 1, using single-point energies of the lowest triplet and broken-symmetry singlet states and their respective $\langle S^2 \rangle$ expectation values. Tight convergence criteria were employed, and atomic coordinates were taken from the 100 K crystallographic data. The geometry of the model radical **2** ($R_1 = R_2 = H$) was taken from a fully optimized (in C_{2v} symmetry) calculation at the UB3LYP/6-31G(d,p) level. Exchange energies were then calculated every 0.1 Å over the range r = 1.5−3.0 Å using a fixed δ = 3.45 Å.

Acknowledgment. We thank the Natural Sciences and Engineering Research Council of Canada (NSERCC) for financial support. We acknowledge the NSERCC for a Canada Graduate Scholarship to A.A.L., the Ontario Government for a Graduate Scholarship to C.M.R., and the Canada Council for the Arts for a Killam Research Fellowship to R.T.O. We are indebted to Dr. Richard Smith for ESI-MS analyses.

Supporting Information Available: Complete refs 4, 23b, and 53; details of X-ray crystallographic data collection and structure refinement at ambient temperature and 100 K; tables of atomic coordinates, bond distances and angles, anisotropic thermal parameters, and hydrogen atom positions (in CIF format); summaries of DFT calculations of magnetic exchange interactions. This information is available free of charge via the Internet at http://pubs.acs.org.

JA8054436

(43) Boeré, R. T.; Moock, K. H.; Parvez, M. *Z. Anorg. Allg. Chem.* **1994**, *620*, 1589.
(44) *SAINT*, version 6.22; Bruker Advanced X-ray Solutions, Inc.: Madison, WI, 2001.
(45) Sheldrick, G. M. *Acta Crystallogr. A* **1990**, *46*, 467.
(46) Sheldrick, G. M. *SHELXL-97*, Program for the Refinement of Crystal Structures; University of Gottingen: Gottingen, Germany, 1997.
(47) *SHELXTL*, Version 6.12 Program Library for Structure Solution and Molecular Graphics; Bruker Advanced X-ray Solutions, Inc.: Madison, WI, 2001.
(48) *EHMACC*, Quantum Chemistry Program Exchange, program no. 571.
(49) Basch, H.; Viste, A.; Gray, H. B. *Theor. Chim. Acta* **1965**, *3*, 458.
(50) Clementi, E.; Roetti, C. *At. Data Nucl. Data Tables* **1974**, *14*, 177.
(51) Hinze, J.; Jaffe, H. H. *J. Chem. Phys.* **1963**, *67*, 1501.
(52) Ammeter, J. H.; Bürgi, H. B.; Thibeault, J. C.; Hoffmann, R. *J. Am. Chem. Soc.* **1978**, *100*, 3686.
(53) Frisch, M. J.; et al. *Gaussian 03*, Revision C.02; Gaussian, Inc.: Wallingford, CT, 2004.